Colossal Magnetoresistance Without Mn^{3+}/Mn^{4+} Double Exchange in the Stoichiometric Pyrochlore $Tl_2Mn_2O_7$

M. A. Subramanian,* B. H. Toby, A. P. Ramirez, W. J. Marshall, A. W. Sleight, G. H. Kwei

Structural analysis from powder neutron and single-crystal x-ray diffraction data for a sample of the $Tl_2Mn_2O_7$ pyrochlore, which exhibits colossal magnetoresistance (CMR), shows no deviations from ideal stoichiometry. This analysis gives an Mn-O distance of 1.90 angstroms, which is significantly shorter than the Mn-O distances (1.94 to 2.00 angstroms) observed in phases based on $LaMnO_3$ perovskites that exhibit CMR. Both results in $Tl_2Mn_2O_7$ indicate oxidation states very close to $Tl_2^{3+}Mn_2^{4+}O_7$. Thus, $Tl_2Mn_2O_7$ has neither mixed valence for a double-exchange magnetic interaction nor a Jahn-Teller cation such as Mn^{3+}, both of which were thought to have an important function in CMR materials. An alternate mechanism for CMR in $Tl_2Mn_2O_7$ based on magnetic ordering driven by superexchange and strong spin-fluctuation scattering above the Curie temperature is proposed here.

The strong correlation between magnetic moment and electrical resistance and the resulting large magnetoresistance near room temperature in lanthanum manganese oxides ($La_{1-x}M_xMnO_3$, where M = Ca, Sr, or Ba) is well known (*1*). Recently, nearly 100% suppression of the resistance was observed in thin films of manganite in a field of 6 T (*2*), and the possible use of this effect for reading magnetic storage media has increased interest in these materials. The fundamental interaction in these manganese oxide materials is double exchange (DE), where electronic carrier hopping between heterovalent Mn pairs (Mn^{3+}/Mn^{4+} in the case of $La_{1-x}M_xMnO_3$) is enhanced by the mutual alignment of the two magnetic moments. A ferromagnetic (FM) transition is stabilized by the kinetic energy gain of the carriers when a transition occurs from incoherent hopping to metallic conduction (*3*). The high resistivity at temperatures above the FM transition, and thus ultimately CMR in $La_{1-x}M_xMnO_3$, is explained by the strong Jahn-Teller effect in these compounds (*4*). Although both heterovalence and strong Jahn-Teller effects are necessary to produce CMR in the $La_{1-xR}M_xMnO_3$ compounds, CMR-type magnetoresistance is found in other systems but at much lower temperatures. Perhaps the best known example of this is $Eu_{0.95}Gd_{0.05}Se$ with a critical temperature (T_c) ≈ 20 K (*5*). Here, CMR is not driven by the same interatomic DE mechanism as are the manganese oxides but rather by an intra-atomic version of the process. We present evidence here for a different mechanism that leads to CMR in $Tl_2Mn_2O_7$ at high temperatures.

The $La_{1-x}A_x^{2+}MnO_3$ materials showing CMR have a perovskite structure. Recently, comparable CMR has been found for $Tl_2Mn_2O_7$ (*6*), which has a pyrochlore structure (*7*) (Fig. 1). Because $Tl_2Mn_2O_7$ also contains Mn as the magnetic constituent, it was thought that this compound would also contain significant amounts of the Jahn-Teller cation Mn^{3+} and that it was again Mn^{3+}/Mn^{4+} DE that gave rise to ferromagnetism. Mixed valence could result from oxygen deficiency (*6*); in fact, the lattice constant of $Tl_2Mn_2O_7$ is greater than expected when compared to that in the isostructural compounds, where Tl is completely replaced by a rare earth ion. The larger lattice constant could result from the formulation $Tl_2Mn^{4+}_{2-2x}Mn^{3+}_{2x}O_{7-x}$ because Mn^{3+} is significantly larger than Mn^{4+} and oxygen deficiency is well established in many compounds with the pyrochlore structure (*7*). However, our structural analysis on $Tl_2Mn_2O_7$ indicates negligible oxygen deficiency and an Mn-O distance inconsistent with a mixture of Mn^{3+} and Mn^{4+}. Thus, the accepted theoretical description for CMR in the perovskites is unlikely to be applicable in these systems. We report results of neutron powder and single-crystal x-ray diffraction (XRD) measurements and transport data for $Tl_2Mn_2O_7$ that provide the structure, oxygen stoichiometry, and magnetic moment in this material. These results show that the pyrochlores represent a distinct class of CMR materials, with magnetic ordering driven by superexchange rather than by DE.

Appropriate quantities of high-purity Tl_2O_3 and MnO_2 were mixed together in an agate mortar and sealed in a gold capsule. The capsule was heated to 850°C for 30 min at a pressure of 58 kbar in a tetrahedral anvil press and was then rapidly cooled to room temperature before the pressure was released (*8*). The powder XRD pattern for $Tl_2Mn_2O_7$ showed that all observed peaks could be indexed with a cubic cell with a = 9.890 ± 0.001 Å and space group $Fd\bar{3}m$. The resistivity as a function of temperature, $\rho(T)$ (*9*), for the $Tl_2Mn_2O_7$ samples used in this study (Fig. 2A) are comparable to those reported recently (*6*). A sharp decrease in $\rho(T)$ occurred at the

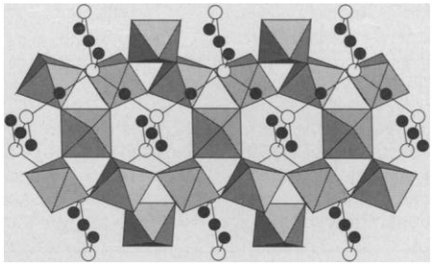

Fig. 1. Schematic view of the structure of $Tl_2Mn_2O_7$, emphasizing the structural arrangement of the MnO_{II}^6 octahedra. Corner-shared oxygens connect the octahedra, forming an Mn-O-Mn bond angle of about 134°. Small filled circles represent Tl ions, and the large open circles represent the O^I oxygens.

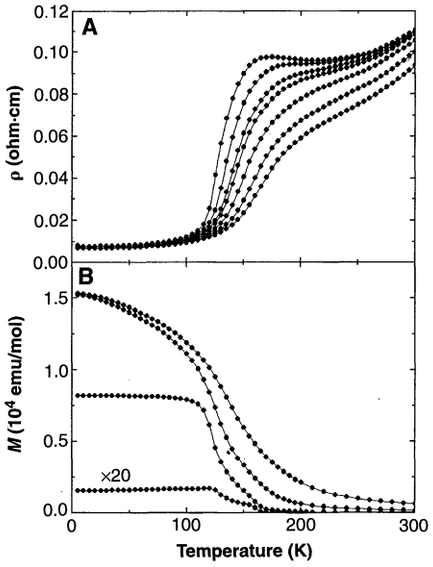

Fig. 2. Temperature dependence of the (**A**) resistivity and (**B**) magnetization for $Tl_2Mn_2O_7$. The resistivity data are (from top to bottom) for 0, 0.1, 1, 2, 4, 6, and 8 T. The magnetization data are (from bottom to top) for 0.001, 0.1, 1, and 4 T.

M. A. Subramanian and W. J. Marshall, Dupont Central Research and Development, Experimental Station, Wilmington, DE 19880–0328, USA.
B. H. Toby, Reactor Radiation Division, National Institute of Standards and Technology, Gaithersburg, MD 20899, USA.
A. P. Ramirez, Bell Laboratories, Lucent Technologies, 600 Mountain Avenue, Murray Hill, NJ 07974, USA.
A. W. Sleight, Department of Chemistry, Oregon State University, Corvallis, OR 97331, USA.
G. H. Kwei, Chemistry and Materials Sciences Department, Lawrence Livermore National Laboratory, Livermore, CA 94550, USA.

*To whom correspondence should be addressed.

zero-field FM transition $T_c(H = 0) \approx 142$ K, and a maximum magnetoresistance between $H = 0$ and 8 T of 60% is comparable to values obtained in the bulk perovskite samples. At 142 K, we saw a rise in dc magnetizaton $M(T)$ and a saturation moment at 10 K and 4 T of 2.74 Bohr magnetons (μ_B) (Fig. 2B), slightly less than that expected for Mn^{4+} (3 μ_B) and consistent with results from a recent study (*6*). This correspondence between a sharp resistance drop and the development of an FM moment is also seen in the perovskites and is the hallmark of CMR compounds.

Neutron powder diffraction data were collected at 298 and 50 K (*10*). In the single-crystal XRD experiments, a full sphere of reflections were collected at 296 K on an Enraf-Nonius CAD-4 diffractometer (MoKα radiation) from a wedge-shaped crystal of approximately 0.04 mm by 0.03 mm by 0.04 mm. The structural refinements from both neutron powder and x-ray single crystal diffraction data (*11*) gave similar lattice and positional parameters (Table 1) and hence similar bond distances and angles (Table 2).

The structure of $Tl_2Mn_2O_7$ (Fig. 1) is based on a network of corner-sharing MnO_6 octahedra, just as in the case of perovskite $CaMnO_3$. However, the manner of linking octahedra leads to Mn-O-Mn angles in the range close to 180° in the perovskite structure (for $La_{1-x}Ca_xMnO_3$, this angle is ~160°) but near 134° in the pyrochlore structure. The site symmetry at the Mn site in the pyrochlore structure is $\bar{3}$. Thus, whereas all of the Mn-O distances are equal, the O-Mn-O angles are not constrained to be 90°. The MnO_6 octahedron is distorted and is actually a trigonal antiprism, as it is in all compounds with the pyrochlore structure. This distortion is, however, not a Jahn-Teller type distortion, where opposite bonds lengthen or shorten relative to others (*12*). The $A_2M_2O_7$ pyrochlore structure may be viewed as two interpenetrating networks: one with the formula MO_3^{II} and the other with the formula A_2O^{I}. Because the MO_3 network forms the backbone of the pyrochlore structure, vacancies can occur only on the A and O^{I} sites (*7*). For this reason, our structural analysis of $Tl_2Mn_2O_7$ focused on both Tl and O^{I} vacancies.

The refinement of occupation parameters in $Tl_2Mn_2O_7$ confirms the ideal stoichiometry within our experimental accuracy (*13*). Conservative estimates are that there could be no more than 1% of the Tl sites vacant or 3.5% of O^{I} sites vacant. This conclusion is further supported by the refined Mn-O distance of 1.90 Å. This is the Mn-O distance expected on the basis of the ionic radii sum of Mn^{4+} and O^{2-} (*14*). A considerably longer distance would be expected if there were large amounts of Mn^{3+} substituting for Mn^{4+} in $Tl_2Mn_2O_7$. Thus, in the $La_{1-x}A_x^{2+}MnO_3$ perovskites with mixed Mn^{3+}/Mn^{4+} valence, the Mn-O distances range from 1.94 to 2.00 Å. Structural analysis of insulating $Er_2Mn_2O_7$ and $Y_2Mn_2O_7$ pyrochlores showed ideal stoichiometries with Mn-O distances of 1.91 Å in cases where the Mn valence must be 4+ (*12*). The Mn-O distance in $Tl_2Mn_2O_7$ may be slightly less than that in rare earth pyrochlores (Table 3). If some mixed valence exists in $Tl_2Mn_2O_7$, it is more likely to be Mn^{5+}/Mn^{4+} than Mn^{3+}/Mn^{4+}. This mixing could occur in stoichiometric $Tl_2Mn_2O_7$ if the Tl 6*s* band overlaps the Mn 3*d* band.

Despite the small Mn-O distance in $Tl_2Mn_2O_7$, the lattice constant of this compound is unexpectedly large when compared to that in the analogous rare earth pyrochlores; the same anomaly is found for $Tl_2Ru_2O_7$ and $Tl_2Ir_2O_7$ (Fig. 3). For the $A_2Mn_2O_7$, $A_2Ru_2O_7$, and $A_2Ir_2O_7$ pyrochlores, semiconducting properties are observed when A is a rare earth element, but metallic properties are observed when A is Tl (*12*, *15*). However, for $A_2Pt_2O_7$ pyrochlores, semiconducting properties are observed even for $Tl_2Pt_2O_7$, which has a normal lattice constant. The metallic conductivity and the anomalous lattice constants for $Tl_2Ru_2O_7$ and $Tl_2Ir_2O_7$ can be ex-

Table 2. Selected bond distances and angles for $Tl_2Mn_2O_7$ from neutron powder (T = 50 and 298 K) and x-ray single-crystal (296 K) diffraction measurements.

Data set	Distance (Å)			Angle (degrees)	
	Tl-O^{I}	Tl-O^{II}	Mn-O^{II}	O^{II}-Mn-O^{II}	Mn-O^{II}-Mn
			Neutron powder		
50 K	2.1395(1)	2.455(2)	1.8993(11)	85.0(1), 95.0(1), 180	133.8(2)
298 K	2.1418(1)	2.463(2)	1.8986(13)	85.2(1), 94.7(1), 180	134.2(2)
			X-ray diffraction		
296 K	2.1417(2)	2.458(5)	1.901(3)	85.0(3), 95.0(3), 180	133.8(4)

Table 3. Comparison of the observed lattice parameters (Å), bond distances (Å), and Mn-O^{II}-Mn bond angles (degrees) in several cubic $A_2Mn_2O_7$ pyrochlores. Values for A = Er and Y are from (*12*); values of the ionic radii for VIII-fold coordinated A^{3+} are from (*14*).

Parameter	$Tl_2Mn_2O_7$	$Er_2Mn_2O_7$	$Y_2Mn_2O_7$
Lattice parameter	9.892(1)	9.875(1)	9.902(1)
Mn-O^{II} (x6)	1.901(3)	1.908(1)	1.911(1)
Tl-O^{II} (x6)	2.458(5)	2.435(6)	2.447(6)
Tl-O^{I} (x2)	2.1417(2)	2.1380(5)	2.1439(1)
Mn-O^{II}-Mn	133.8(4)	132.3	132.7
Ionic radius of A^{3+}	0.98	1.004	1.019

Table 1. Structural parameters for $Tl_2Mn_2O_7$ (space group $Fd\bar{3}m$) from neutron powder (T = 50 and 298 K) and single-crystal x-ray (296 K) diffraction measurements. Numbers in parentheses after the refined parameters represent 1σ in the last digits. The lattice parameter is denoted by *a*, and the atomic position of O^{II} is denoted as a fractional coordinate by *x*. The thermal factors are given in units of 1000 Å^2. The values of U_{eqv} from single-crystal x-ray refinements are taken as one-third of the trace of the refined unconstrained thermal factor tensor. The refinement of site occupancies is discussed in (*13*). Atomic positions are as follows: Tl 16*d*(½,½,½); Mn 16*c*(0,0,0); O^{I} 8*b*(⅜,⅜,⅜); and O^{II} 48*f* (*x*,⅛,⅛).

Parameter	*a* (Å)	*x* [O(II)]	U_{iso} or U_{eqv}				Site occupancy	
			Tl	Mn	O^{I}	O^{II}	Tl	O^{I}
50 K	9.8819(1)	0.3254(3)	4.9(8)	4.5(14)	1.8(12)	8.1(6)	1	1
298 K	9.8927(3)	0.3250(4)	8.1(11)	7.5(20)	5.8(17)	9.8(8)	1	1
X-ray	9.892(1)	0.3254(8)	6	6	4	9	1.000(12)	0.972(17)

plained by the overlap of the Tl 6*s* band with either the Ru 4*d* band or the Ir 5*d* band. In chemical terms, this overlap means reduction of Tl and oxidation of Ru or Ir. Oxidation of the 4+ cations leads to a small reduction in the M-O bond length, and reduction of Tl^{3+} causes a disproportionate increase in the Tl-O bond length. The net effect is that the lattice constant of $Tl^{3+}_{2-x}Tl^{2+}_{x}Mn^{4+}_{2-x}Mn^{5+}_{x}O_7$ increases as *x* increases. Although Tl^{2+} is not a normal oxidation state of Tl, this is inconsequential if the electron associated with Tl reduction is actually delocalized in a Tl 6*s* band.

Hall effect data on $Tl_2Mn_2O_7$ indicate a small number of high-mobility *n*-type carriers (6). This would not be expected from an Mn 3*d* band but could result from a small number of carriers in the Tl 6*s* band. These carriers could be produced by $Tl^{3+}_{2-x}Tl^{2+}_{x}Mn^{4+}_{2-x}Mn^{5+}_{x}O_7$ or by $Tl^{3+}_{2-y}Tl^{2+}_{y}Mn^{4+}_{2}O_{7-y/2}$. The value of *x* or *y* would need to be only ~0.005 to explain the Hall data, and neither of these values would be inconsistent with our measured stoichiometry.

Cooling $Tl_2Mn_2O_7$ to 50 K leads to a 30% increase in the relative intensity of the (111) reflection in the neutron diffraction pattern (*16*). Thus, a refinement of the magnetic contribution was possible, which gave a magnetic moment of 2.5 ± 0.2 μ_B per Mn. This value is in good agreement with the value of 2.74 μ_B from our magnetization measurements as well as with the value of 2.59 μ_B from the earlier measurement on a sample containing a small amount of impurity (6). The orientation of the magnetic vector with respect to the lattice cannot be determined from powder neutron diffraction data (*17*).

The FM pyrochlore compound $Tl_2Mn_2O_7$ bears more than superficial similarity to the CMR manganese oxide perovskite compounds. Both compounds are oxides, and both have strong local moment magnetism arising from octahedrally coordinated Mn. Both exhibit dramatic decreases in the resistivity associated with the transition from the high-temperature paramagnetic state to the low-temperature FM state and the associated CMR. Because of these observed similarities between macroscopic and microscopic properties, one might argue that the underlying mechanism for the FM transition is the same in both cases: namely, one driven by DE among heterovalent Mn neighbors. However, our results underscore the differences between the two compound families, and these differences strongly suggest that a fundamentally different mechanism drives CMR in the pyrochlore system.

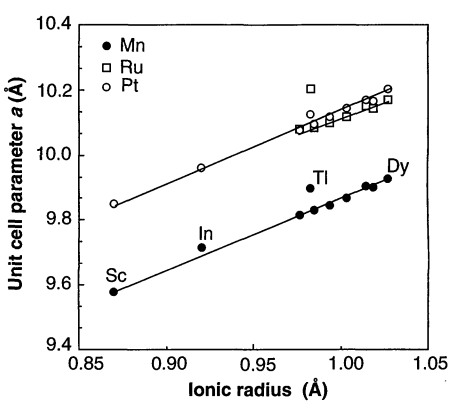

Fig. 3. Plot of ionic radius of A^{3+} cation (VIII-fold coordination) versus cubic unit cell parameter *a* for $A_2M_2O_7$ pyrochlores (A = Dy-Lu, Y, In, Sc, and Tl; M = Mn, Ru, or Pt). The unit cell parameter values are taken from (*7*) and (*12*) (and references cited therein). The data points for M = Ir also follow the same trend as those for Ru. The ionic radii values are from (*14*).

On a microscopic level, we see no evidence for significant doping in the pyrochlore Mn-O sublattice (*18*). First, such doping is necessary to produce the mixed valence responsible for DE in the perovskites; CMR occurs over the range of 20 to 45% of hole concentrations (with respect to Mn), obtained by doping with an alkaline earth on the rare earth site (*19*). Second, there is no evidence for Jahn-Teller distortions among the Mn-O octahedra, which is consistent with the stoichiometry of the compound and the approximately homovalent Mn population thus implied. Third, the above-mentioned tendency for Tl to form 6*s* conduction bands is unlike the perovskite case, where the rare earth levels are inactive electronically. From a macroscopic perspective, the saturation moment of 2.74 μ_B is below the value expected for Mn^{4+}, which is consistent with an absence of Mn^{3+} and the weakly covalent character among the Mn valence electrons. Finally, the resistivity of $Tl_2Mn_2O_7$ in the paramagnetic state is metal-like ($d\rho/dT > 0$), which is unlike the perovskites, where polycrystalline samples typically exhibit hopping-type conductivity ($d\rho/dT < 0$).

Compounds with a pyrochlore structure cannot exhibit simple antiferromagnetism because the tetrahedral arrangement of metal cations gives rise to classic frustration. In addition, FM exchange interactions between metal cations become significant in the d^3 situation as the metal-O-metal bond angle bends appreciably away from 180° (*20*). For perovskites, there is no frustration, metal-O-metal angles are near 180°, and FM insulators are rare. Indeed, the end members of the CMR perovskites, $LaMnO_3$ and $CaMnO_3$, are both anti-FM superexchange insulators. Coexisting with this superexchange interaction in $Tl_2Mn_2O_7$ is a Tl-based conduction band. In a stoichiometric compound, overlap of the Tl 6*s* band with the Mn 3*d* band would lead to valence mixing in the Mn sublattice—hence, the possibility of DE between Mn^{4+}/Mn^{5+} pairs. We believe, however, that Tl 6*s*–Mn 3*d* overlap is insufficient to produce DE involving Mn^{4+}/Mn^{5+} given (i) the apparently very small number of carriers in the Tl 6*s* band, (ii) the unstable nature of the Mn^{5+} ion, (iii) a resulting hopping-transfer integral much reduced from that seen in the Mn^{3+}/Mn^{4+} perovskites, and (iv) a density of such pairs well below the percolation limit for nearest neighbor hopping in the pyrochlore structure.

We propose that the origin of CMR in $Tl_2Mn_2O_7$ is fundamentally different from that of the perovskites. Instead of a single mechanism (DE) driving both the conduction and the magnetic ordering processes, as in the perovskites, there are two processes in the pyrochlore compound. The magnetic ordering seems to be driven by superexchange, as in other FM pyrochlore insulators. The conduction band, however, most likely involves a large admixture of Tl-based valence states. The interdependence of ρ and M results from unusually large, incoherent scattering from spin fluctuations accompanying FM ordering in a relaxation-time approximation (*21*). Given such interdependence, CMR results from the field-dependence of T_c, $dT_c/dH > 0$, which is similar to that in the perovskite compounds. This realization of a new route to CMR permits the engineering of new materials for eventual use in magnetic reading applications.

REFERENCES AND NOTES

1. G. H. Jonker and J. H. Van Santen, *Physica* **16**, 337 (1950); G. H. Jonker, *ibid.* **22**, 707 (1956); J. Volger, *ibid.* **20**, 49 (1954); C. W. Searle and S. T. Wang, *Can. J. Phys.* **47**, 2703 (1969); *ibid.* **48**, 2023 (1970).
2. S. Jin *et al.*, *Science* **264**, 413 (1994).
3. C. Zener, *Phys. Rev.* **82**, 403 (1951); P. W. Anderson and H. Hasegawa, *ibid.* **100**, 675 (1955); P.-G. de Gennes, *ibid.* **118**, 141 (1960).
4. N.-L. H. Liu and D. Emin, *Phys. Rev. Lett.* **42**, 71 (1979); A. J. Millis, P. B. Littlewood, B. I. Shraiman, *ibid.* **74**, 5144 (1995); H. Röder, J. Zhang, A. R. Bishop, *ibid.* **76**, 1356 (1996).
5. S. von Molnar and S. Methfessel, *J. Appl. Phys.* **38**, 959 (1967).
6. Y. Shimakawa, Y. Kubo, T. Manako, *Nature* **379**, 53 (1996).
7. M. A. Subramanian, G. Aravamudan, G. V. Subba Rao, *Prog. Solid State Chem.* **15**, 55 (1983); H. Fujinaka *et al.*, *Mater. Res. Bull.* **14**, 1133 (1979); N. P. Raju, J. E. Greedan, M. A. Subramanian, *Phys. Rev. B* **49**, 1086 (1994).
8. The sample was weighed before and after the reaction to check for thallium evaporation; the results showed virtually no weight change. Microprobe analysis showed that the Mn:Tl ratio is 0.99 ± 0.01. No reflections due to impurities were observed in the powder XRD pattern. Microscopic examination of the pellet revealed the formation of several small single crystals, which were mechanically removed and used for the single-crystal XRD studies.
9. The dc magnetization *M* was measured as a function of temperature with a commercial superconducting

quantum interference device (SQUID) magnetometer between 5 and 300 K and for magnetic fields up to 4 T. The resistivity (ρ) was measured by a standard in-line, four-probe technique and a commercial ac resistance bridge (operating at 16 Hz) at temperatures between 5 and 300 K and at magnetic fields up to 8 T.
10. Data were collected at 298 and 50 K with a Cu(220) monochromator (wavelength λ = 1.5543 Å) and a Cu(311) monochromator (λ = 1.5396 Å), respectively, on the 32-detector BT-1 diffractometer at the National Institute of Standards and Technology's research reactor. A figure containing the 50 K data with a fitted profile from Rietveld refinement is available at http://www.sciencemag.org/science/feature/beyond/#subramanian. The neutron sample was a pellet weighing 185 mg, which was loaded into a vanadium tube and positioned in the center of the neutron beam. For the 298 K neutron data set, aluminum in the sample mount was incompletely shielded. The resulting aluminum peaks were fit as a second phase with a Le Bail fit [A. Le Bail, H. Duroy, J. L. Fourquet, *Mater. Res. Bull.* **23**, 447 (1988)]. At both temperatures, small peaks from vanadium scattering were also observed and were modeled as an additional phase.
11. A. C. Larson and R. B. Von Dreele, *Rep. LA-UR-86-748* (Los Alamos National Laboratory, Los Alamos, NM, 1986). Refinement statistics for the neutron data at 50 and 298 K are as follows: χ^2 = 0.819 and 0.936, R_{wp} = 7.7 and 3.8%, and R_{exp} = 6.2 and 3.2%, for 69 and 65 unique reflections, respectively. The single-crystal XRD refinement with full anisotropic thermal factors, anomalous scattering terms for Tl and Mn, and no absorption correction (19% variation in the azimuthal scan) gave R_w = 1.3% and R = 1.6%, with 60 unique reflections (>3σ).
12. M. A. Subramanian *et al.*, *J. Solid State Chem.* **72**, 24 (1988).
13. When we used an anisotropic thermal factor model and fixed the Mn and O^{II} occupancies at 1, refinement for Tl and O^{I} site occupancies from x-ray single-crystal refinements resulted in nearly ideal occupancies, giving a composition of $Tl_{2.000(12)}Mn_2O^{I}_6O^{II}_{0.972(17)}$ (numbers in parentheses indicate the error in the last digits). In the neutron refinements, it was not possible to simultaneously vary thermal factors and occupancies; thus, these occupancies were set to unity in the refinements. However, a conservative lower limit on the O^{I} site occupancy is 0.965 because smaller values result in negative thermal factors. We conclude that there are no Tl or O^{I} vacancies within the accuracy of the experimental measurements.
14. R. D. Shannon, *Acta Crystallogr. A* **32**, 751 (1976).
15. H. S. Jarrett *et al.*, in *Valence Instabilities and Related Narrow Band Phenomena*, R. D. Parks, Ed. (Plenum, New York, 1977), p. 545; M. A. Subramanian and A. W. Sleight, in *Handbook on the Physics and Chemistry of Rare Earths*, K. A. Gschneider Jr. and L. Eyring, Eds. (Elsevier, Amsterdam, 1993), vol. 10, p. 225.
16. E. O. Wollan and W. C. Koehler [*Phys. Rev.* **100**, 545 (1955)] and Z. Jirák, S. Krupicka, Z. Simsa, M. Dlouá, and S. Vratislav [*J. Magn. Magn. Mater.* **53**, 153 (1985)], for example, have reported such magnetic structure determinations for a number of manganese oxide perovskites.
17. G. Shirane, *Acta Crystallogr.* **12**, 282 (1959).
18. We have recently obtained data that substantiate this lack of significant doping through an x-ray absorption near-edge spectroscopy (Mn K edge) study of $Tl_2Mn_2O_7$ (H. D. Rosenfeld and M. A. Subramanian, unpublished material). The Mn K edge of $Tl_2Mn_2O_7$ coincides with the K edges observed for $Mn^{4+}O_2$ and pyrochlore $Er_2Mn^{4+}_2O_7$, both containing only Mn^{4+}. In addition, the K edge of $Tl_2Mn_2O_7$ also shows appropriate shifts from the K edges observed for $Mn^{3+}_2O_3$ and CMR perovskite $La^{3+}_{0.7}Sr^{2+}_{0.3}Mn^{3.3+}O_3$.
19. P. Shiffer, A. P. Ramirez, W. Bao, S.-W. Cheong, *Phys. Rev. Lett.* **75**, 3336 (1995).
20. J. B. Goodenough, *Magnetism and the Chemical Bond* (Krieger, New York, 1976), p. 184.
21. M. E. Fisher and J. S. Langer, *Phys. Rev. Lett.* **20**, 665 (1968).
22. We thank Q. Z. Huang, M. K. Crawford, J. E. Greedan, A. C. Larson, and C. Broholm for useful discussions on the magnetic refinements, R. L. Harlow for help in the single-crystal work, and T. G. Calvarese and M. L. Plummer for help in the high-pressure synthesis. The work at Lawrence Livermore was done under the auspices of the U.S. Department of Energy under contract W-7405-ENG-48. A.W.S. thanks NSF for research grant DMR-9308530.

18 March 1996; accepted 29 May 1996

Direct, Nondestructive Observation of a Bose Condensate

M. R. Andrews, M.-O. Mewes, N. J. van Druten, D. S. Durfee, D. M. Kurn, W. Ketterle

The spatial observation of a Bose condensate is reported. Dispersive light scattering was used to observe the separation between the condensed and normal components of the Bose gas inside a magnetic trap. This technique is nondestructive, and about a hundred images of the same condensate can be taken. The width of the angular distribution of scattered light increased suddenly at the phase transition.

Bose-Einstein condensation (BEC) is characterized by a macroscopic population of particles in the quantum-mechanical ground state below a critical temperature. It is the origin of macroscopic quantum phenomena such as superfluidity in liquid helium (*1*). For a homogeneous sample, BEC is sometimes called "condensation in momentum space" (*2*) because it does not lead to a spatial separation between the condensate and the normal component. However, in any inhomogeneous potential—for example, in atom traps or even in Earth's gravitational field—the condensate and the normal fraction of a Bose gas are spatially separated (*2*, *3*). So far, BEC has only been seen in momentum space: the condensate fraction of liquid helium was determined by neutron scattering (*4*), the condensation of excitons was deduced from the observed energy distribution of the excitonic particles (*5*), and BEC in dilute atomic gases was detected by observation of the velocity distribution of freely expanding Bose condensates (*6*, *7*). We report the direct and nondestructive observation of the spatially localized condensate in a gas of magnetically trapped sodium atoms.

Bose condensates of dilute atomic gases are a new form of quantum matter. The pioneering work toward BEC in atomic gases was done with spin-polarized hydrogen with the use of magnetic trapping and evaporative cooling (*8*). In work at JILA (*9*) and the Massachusetts Institute of Technology (*10*), these techniques were successfully combined with laser cooling (*11*), which resulted in the observation of BEC in rubidium in June (*6*) and in sodium in September of 1995 (*7*). Lithium has also been cooled to the quantum degenerate regime (*12*). Since these developments, there has been a flurry of both theoretical and experimental activity (*13*).

In atom traps, the condensation phenomenon results in the formation of a dense core of atoms in the ground state of the system surrounded by the normal component—analogous to droplet formation in a saturated vapor. Our earlier attempts to observe the Bose condensate directly by absorption imaging failed because of the high optical density of the atom cloud near the critical temperature. For typical parameters of our experiment, the peak optical density D_0 for resonant light was about 300, corresponding to a transmission coefficient of e^{-300}. Thus, the probe light was completely absorbed, even in the wings of the spatial distribution, preventing direct imaging of the condensate. Detuning of the light, which reduced the absorption, revealed major image distortions caused by dispersive effects: the condensate acted as a lens and strongly deflected the light. However, by using the so-called "dark-ground" imaging technique (*14*), we were able to use the dispersively scattered light to clearly image the condensate.

Dispersive imaging has significant advantages over absorption methods for the imaging of small and dense clouds ($D_0 \gg 1$). To obtain a good absorption signal, one would like to detune the probe light until the off-resonant optical density D is close to unity; D is given by $D = D_0/\Delta^2$, where the detuning Δ from the resonant frequency ω_0 is $\Delta = 2(\omega - \omega_0)/\Gamma$, with Γ being the natural linewidth. The maximum phase shift δ of the transmitted wave is $\delta = D_0/2\Delta$, and thus for $D \sim 1$, the phase shift is $\delta \sim \sqrt{D_0}/2$. Such a large phase shift is caused by lenslike refraction, which bends

Department of Physics and Research Laboratory of Electronics, Massachusetts Institute of Technology, Cambridge, MA 02139, USA.